

PAPER

Design, fabrication and skin-electrode contact analysis of polymer microneedle-based ECG electrodes

To cite this article: Conor O'Mahony *et al* 2016 *J. Micromech. Microeng.* **26** 084005

View the [article online](#) for updates and enhancements.

You may also like

- [Development of Low Cost Rapid Fabrication of Sharp Polymer Microneedles for In Vivo Glucose Biosensing Applications](#)
Colm Barrett, Karen Dawson, Conor O'Mahony et al.
- [Piezoelectric inkjet coating of injection moulded, reservoir-tipped microneedle arrays for transdermal delivery](#)
Conor O'Mahony, Andrea Bocchino, Michael J Haslinger et al.
- [Recent advances on fabrication of microneedles on the flexible substrate](#)
Dong Huang, Junshi Li, Tingyu Li et al.



ECS
The
Electrochemical
Society
Advancing solid state &
electrochemical science & technology

DISCOVER
how sustainability
intersects with
electrochemistry & solid
state science research

Design, fabrication and skin-electrode contact analysis of polymer microneedle-based ECG electrodes

Conor O'Mahony¹, Konstantin Grygoryev¹, Antonio Ciarlone^{1,2}, Giuseppe Giannoni^{1,2}, Anan Kenthao^{1,3} and Paul Galvin¹

¹ Tyndall National Institute, University College Cork, Cork, Ireland

² Dipartimento di Elettronica e delle Telecomunicazioni, Politecnico di Torino, Torino, Italy

³ Department of Biology, Khon Kaen University, Khon Kaen, Thailand

E-mail: conor.omahony@tyndall.ie

Received 7 January 2016, revised 30 March 2016

Accepted for publication 31 March 2016

Published 22 July 2016



Abstract

Microneedle-based 'dry' electrodes have immense potential for use in diagnostic procedures such as electrocardiography (ECG) analysis, as they eliminate several of the drawbacks associated with the conventional 'wet' electrodes currently used for physiological signal recording. To be commercially successful in such a competitive market, it is essential that dry electrodes are manufacturable in high volumes and at low cost. In addition, the topographical nature of these emerging devices means that electrode performance is likely to be highly dependent on the quality of the skin-electrode contact.

This paper presents a low-cost, wafer-level micromoulding technology for the fabrication of polymeric ECG electrodes that use microneedle structures to make a direct electrical contact to the body. The double-sided moulding process can be used to eliminate post-process via creation and wafer dicing steps. In addition, measurement techniques have been developed to characterize the skin-electrode contact force. We perform the first analysis of signal-to-noise ratio dependency on contact force, and show that although microneedle-based electrodes can outperform conventional gel electrodes, the quality of ECG recordings is significantly dependent on temporal and mechanical aspects of the skin-electrode interface.

Keywords: microneedles, electrode, ECG, polymer, micromoulding, signal-to-noise ratio

(Some figures may appear in colour only in the online journal)

1. Introduction

In common with other organs in the human body, such as the brain, muscles, and eyes, the heart produces measurable electrical signals as a result of its activity. Electrocardiography (ECG) data is commonly recorded during a myriad of clinical procedures in order to monitor patient wellbeing, and provides important diagnostic information regarding, for example, arrhythmias or heart failure [1, 2].

The collection of ECG data requires dedicated signal recording hardware which is usually interfaced to the human body using adhesive electrodes [3]. ECG signals are low amplitude (1 μ V–10 mV) and low bandwidth (1–200 Hz), and at this frequency range, the electrical impedance between

skin and electrode is relatively high due to the presence of the stratum corneum (SC) layer. This outermost layer of skin consists of a 10–20 μ m thick, semipermeable and electrically insulating layer of dead skin cells [4], the presence of which makes it difficult to record biopotentials with high signal-to-noise ratio (SNR).

An electrolytic gel is often used to reduce this SC impedance and to ensure a better interface between skin and electrode. Although cheap and effective for many short-term measurements, such 'wet' electrodes are unsuited to long-term monitoring as the electrolytic gel tends to dry out over time, leading to lower shelf life, higher contact impedance and a subsequent loss of signal quality [5–7]. Skin abrasion is often carried out prior to electrode placement in order to remove the

SC layer and improve skin-electrode contact. This procedure can cause problems with irritation and possible infection, and is uncomfortable for many patients [8]. Due to the presence of inorganic salts, such as silver chloride, patients may experience local skin sensitization to the gel, and as a result some electrodes cannot be used for extended time periods [5, 9].

'Dry' electrodes, which do not use electrolytic gel and are based on capacitive detection rather than an electrochemical electrode-electrolyte interface, are gaining popularity for long-term use [5, 10, 11]. Recent research has suggested that dry electrodes based upon the use of microneedle arrays may prove a viable alternative for long-term physiological recording applications. Microneedles are short (generally <1 mm), sharp, high aspect ratio structures, micromachined using a variety of processes and materials, and originally intended for use in transdermal drug and vaccine delivery [12, 13]. It has been shown that electrically conductive microneedle arrays can pierce the SC layer and make direct contact with the moist epidermal layers directly beneath the skin's surface, thereby reducing skin-electrode impedance and eliminating the need for skin preparation and/or electrolytic gel [14, 15]. Furthermore, their sub-millimetre height ensures that no pain receptors are stimulated, nor is any blood drawn [16]. This minimizes patient discomfort and risk of infection after the electrode is removed [17].

Several examples of silicon microneedle electrodes have already been demonstrated. However, the requirement to have a connection to the outside world on the back of the electrode means that electrical contact must be established between the front and rear surfaces of the electrode. This has previously been done by making contacts on individual microneedle die after wafer singulation [18–20], but this is time consuming and unsuited to volume production. Alternatively, a through-silicon via (TSV) can be made and metal-coated at wafer level after the microneedles are formed [14], although this adds cost by requiring extra time and processing steps. We have previously demonstrated a solution to this problem by developing a double-sided silicon etch process that simultaneously forms a microneedle on one side of the wafer and a through-silicon via for electrical contact on the other [21]. Qualitative comparisons of signals indicate comparable electrode performance between microneedle and commercially available wet electrodes, and specific waveforms in EEG, ECG or EMG signals could be easily distinguished when using a range of silicon electrodes [20, 22–24].

Since recording electrodes are cheap and disposable devices, silicon may be expensive for use in such a commercially competitive market. There is therefore a need for a microneedle-based dry electrode that is fabricated using a process suited to rapid, economical, high-volume manufacture, and a cost effective alternative may be to use a polymer as the base material for the disposable sensors. It has been previously shown that a range of polymers can be used to create microneedle structures [12]. Specifically, polymeric microneedle electrodes have been demonstrated [20, 25, 26], although those arrays were individually fabricated and also relied on post-process steps to electrically connect the front and rear surfaces of the electrodes.

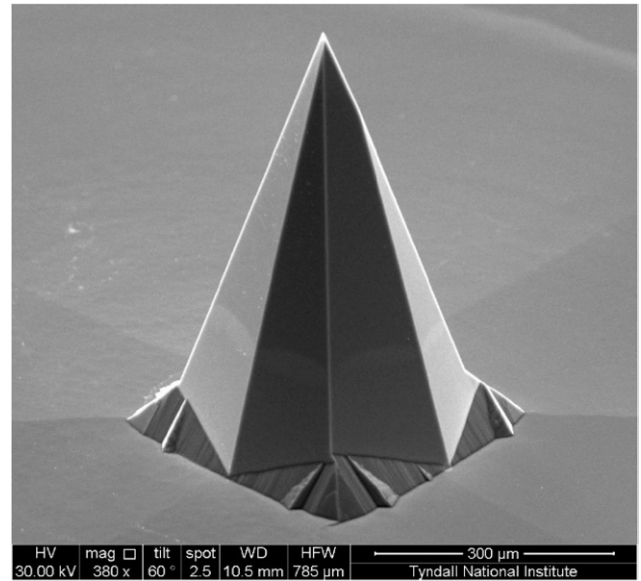


Figure 1. Scanning microscopy image of a $500\ \mu\text{m}$ tall silicon microneedle.

This paper reports on a double-sided, wafer-level micro-moulding process that replicates the silicon microneedle arrays described earlier [21] in low-cost, medical-grade polymeric materials. Two moulds are used to create $500\ \mu\text{m}$ tall microneedle structures on the front side of a polymeric wafer, and to simultaneously define through-wafer electrical vias and circular, detachable arrays on the rear side. The wafers are then metal-coated and interfaced to self-adhesive pads to form ECG electrodes which are capable of accurately measuring the mV-amplitude electrical signals produced by the muscular activity of the heart. This double-sided approach reduces fabrication time and complexity by eliminating the additional processing steps usually required to electrically connect the front and rear of each electrode. It also removes the need for a subsequent wafer dicing step, as the arrays are preformed and easily detached from the polymeric wafer.

Given the topography of the resulting microneedle array surface, it is reasonable to assume that the skin-electrode impedance (and in turn, the fidelity of the recorded signal) is a strong function of the quality of the skin-electrode contact. A number of teams have studied the variation of skin-electrode contact impedance with time and/or applied force [26–30], but to our knowledge no study has yet quantitatively examined the characteristics of the ECG signal obtained using microneedle electrodes as a function of skin contact force.

Therefore, this work has also developed new measurement techniques to characterize the *in situ* skin-electrode contact force, and has carried out the first analysis of SNR dependency on skin-electrode contact quality. By comparing the SNR of commercially-available Ag/AgCl wet electrodes with microneedle electrodes under similar conditions as a function of (i) applied force and (ii) skin contact time, we show that although microneedle-based electrodes can outperform conventional 'wet' electrodes in certain cases, signal fidelity is significantly dependent on the conditions at the skin-electrode interface.

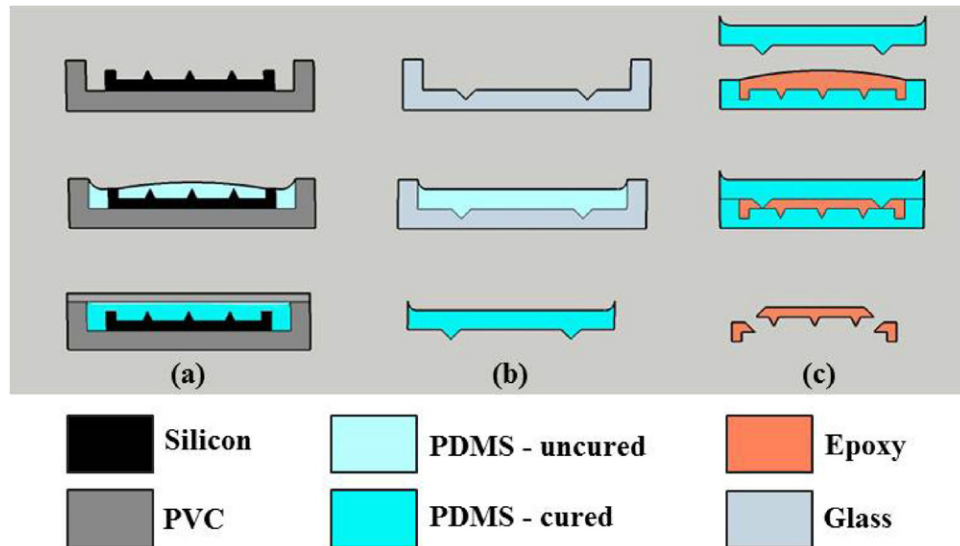


Figure 2. Schematic of microneedle moulding steps. (a) Fabrication of microneedle mould. (b) Fabrication of the array mould. (c) Fabrication of the microneedle arrays using epoxy and two part moulding process.

2. Materials and methods

2.1. Electrode fabrication

Silicon microneedle templates were fabricated using potassium hydroxide (KOH) wet-etching techniques [31]. Square oxide/nitride masks were patterned using standard photolithography tools on boron doped, 100 mm diameter, $\langle 100 \rangle$ monocrystalline silicon wafers. These masks were aligned with the $\langle 110 \rangle$ crystal direction and the height of the subsequent microneedle is a linear function of the mask square side length. The patterned silicon wafer was etched in a 29% w/v aqueous KOH solution until convex corner mask undercut took place, the eight planes intersected and a needle shape was formed, figure 1. This 500 μm tall needle is comprised of eight $\{263\}$ planes, a base of $\{212\}$ planes and has a height:base diameter aspect ratio of 3:2. Tip sharpness is a function of mask and crystal axis alignment accuracy; tip radii are generally of the order of 50–100 nm. Needle-to-needle pitch is 1750 μm .

In order to replicate these silicon wafers in polymeric materials, the wafer was first affixed to a customised holder machined from polyvinyl chloride (PVC) using cyanoacrylate (Super Glue, Loctite, Germany). Medical-grade polydimethylsiloxane (PDMS) (MED-6015, NuSiL Technology, CA, USA), mixed in a 10:1 ratio of elastomer to curing agent, was degassed and poured over the microneedle master template, which was coated with a thin gold layer to assist with demoulding. The elastomer was cured at 100 $^{\circ}\text{C}$ for one hour and peeled from the master wafer when cool.

Polymeric wafers were then fabricated by spreading a biocompatible epoxy (EPO-TEK 353ND, Epoxy Technology, MA, USA) over the PDMS mould; this was left to degas overnight on a vacuum table at room temperature. To simultaneously create through-wafer vias for electrical connectivity and to define the arrays without the need for a post-process wafer dicing step, a secondary mould (also made in PDMS cast from a custom-machined glass template) was pressed into the epoxy to form circular die. The epoxy was then cured

in the oven for a period of 1 h at 90 $^{\circ}\text{C}$. A schematic of the complete process is shown in figure 2, and an image of the micromoulded wafer in figure 3.

The moulded epoxy wafer was then coated on both sides with a 20 nm thick titanium adhesion layer, followed by a 200 nm thick layer of gold. Electrical contact between the front and rear surfaces of the electrodes was established at wafer level through the vias created using the secondary rear mould. Both coatings were deposited using a metal evaporator (Moorfield Nanotechnology, Cheshire, UK) at a rate of 1 $\text{A}^{\circ} \text{s}^{-1}$. Figure 4 illustrates polymeric microneedles after Au coating. Needle tips are generally a little less sharp than the silicon master structures and are typically 1–2 μm in diameter.

To create a wearable prototype, the microneedle arrays were detached from the epoxy wafer shown in figure 3, the electrolytic gel pad was removed from a standard commercial wet electrode (Red Dot 2239 Monitoring Electrode, 3M Healthcare, Germany), and the arrays were affixed in its place using a conductive epoxy (CircuitWorks CW2400, Farnell Element 14, UK). This solution provides both an adhesive backing and a metal snap fastener for connection to recording equipment. For storage purposes, the prototype electrodes were protected by the plastic cover that initially formed part of the commercial electrodes (figure 5), and were UV light sterilized for 30 min. To facilitate an accurate comparison between microneedle-based electrodes (MN) and conventional Red Dot electrodes (RD), the array diameter was chosen to be equal to that of the Red Dot 2239 electrode gel pad, i.e. 18 mm.

2.2. Electrode application force

A flexible, ultrathin resistive force sensor (Flexiforce A201, Tekscan Inc., Boston, USA), with a full scale deflection (FSD) range of 0–5 N, was used to study the influence of skin-electrode contact force on signal quality. This sensor was first calibrated

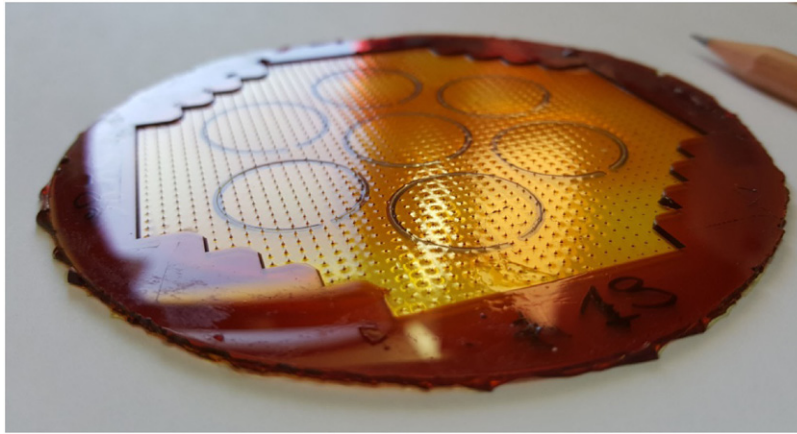


Figure 3. Micromoulded epoxy needle wafer prior to metallisation. Note the circular through-wafer vias that allow electrical contact between the front and rear surfaces, and easy detachment of the electrode arrays from the wafer.

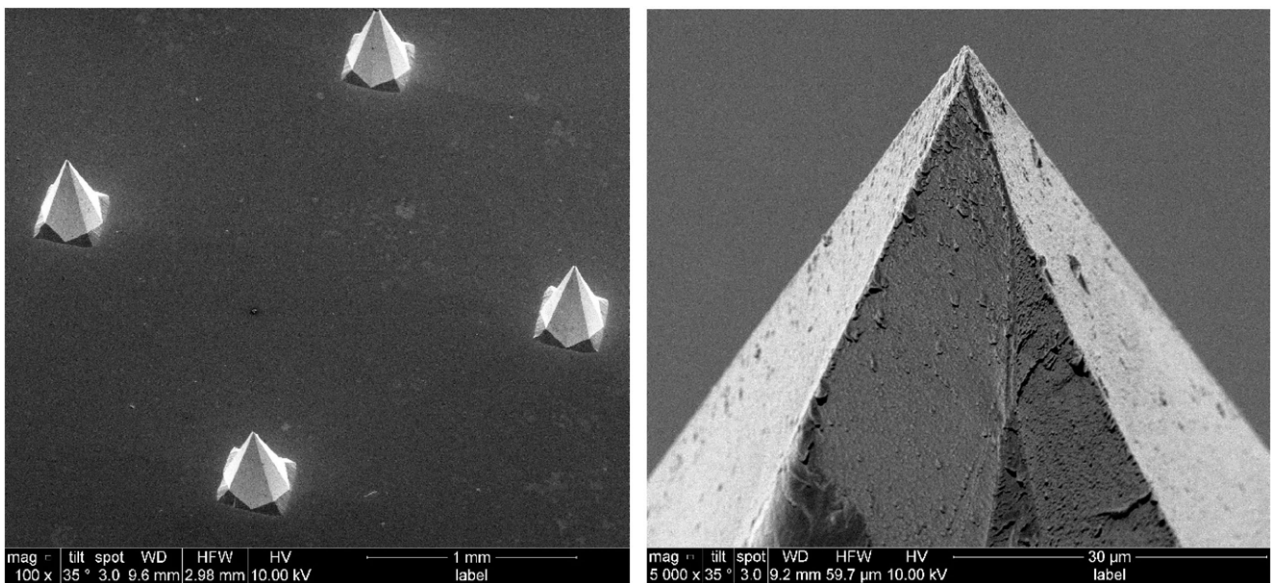


Figure 4. Left: detail of Au coated polymeric microneedle array. Right: close-up of Au coated polymer microneedle tip.

by using a force-displacement test system (Instron 5565, Bucks., UK) to apply a known load to the sensor, and then interfaced to a signal conditioning circuit according to the manufacturer’s instructions [32].

To mimic the conditions at the skin-electrode interface and to spread the load evenly over the sensor, the skin-electrode interface material (gel pad or microneedle array, depending on electrode type) was removed from the electrode and was replaced by a flat, rigid disc of similar dimensions. The Flexiforce sensor was affixed to the upper arm using adhesive tape, and the modified electrode placed over the sensor measurement pad. Output voltage was measured using an Agilent 34411A digital multimeter, which was converted to a force reading using the aforementioned calibration curve. The skin-electrode contact force was then varied by adding or removing up to three layers of an elastic tubular support bandage (Size C Medicgrip, Fleming Medical Ltd, Limerick, Ireland), figure 6. Three readings were taken for each applied force, and this was repeated on three different subjects, i.e. a total of nine readings per layer.

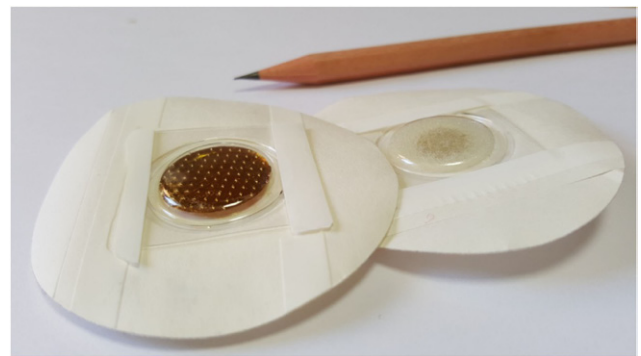


Figure 5. Prototype microneedle-based dry electrode (left) and conventional wet electrode (right). Both electrodes are covered by a protective plastic lid.

2.3. Skin-electrode impedance

Skin-electrode impedance was recorded using a potentiostat/galvanostat (PGSTST 302N, Metrohm Autolab, Utrecht, Netherlands). To analyse the effects of contact force on

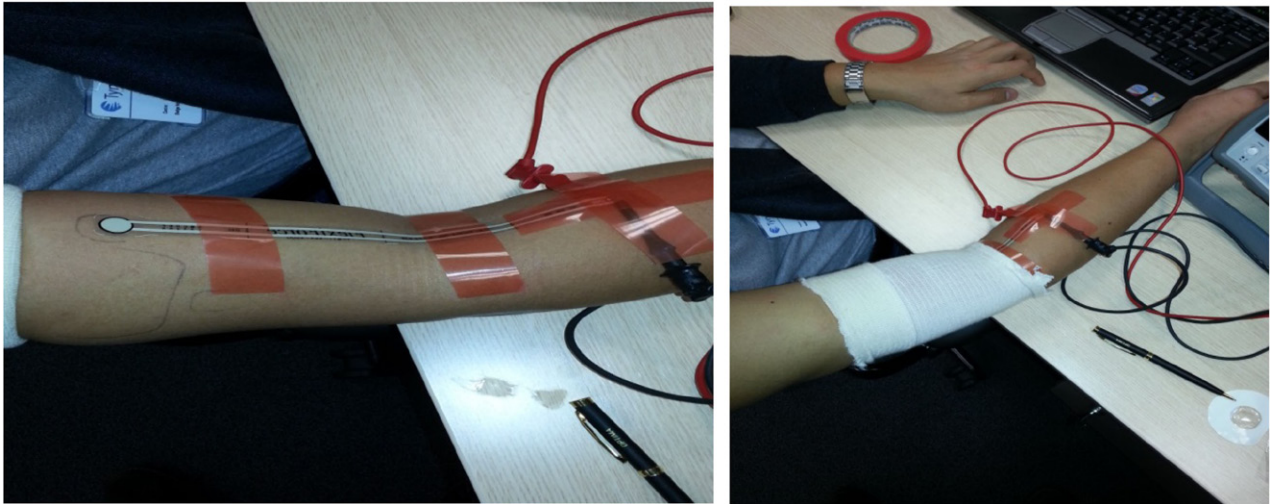


Figure 6. Left: application of force sensor to the upper arm, and (right) increasing skin-electrode force via application of compression bandages.

skin-electrode impedance, pairs of wet Red Dot 2239 and dry microneedle electrodes were attached to a volunteer's forearm, 60 mm apart (centre to centre), and were allowed to equilibrate for 5 min. No skin preparation of any kind (washing, shaving, sanding, abrading) was performed prior to attachment. Similar to figure 6, the number of layers of compression bandage over the electrodes was then increased from zero to three, and decreased back to zero again. At each point a frequency sweep was performed from 1–950 Hz at a voltage bias of 0.2 V and rms amplitude of 0.02 V, and 20 samples per sweep were recorded.

The temporal variation of skin-electrode impedance was also investigated. Pairs of electrodes were applied with a 40 mm centre-to-centre pitch as shown in figure 7. An impedance frequency sweep was performed immediately after electrode application, and then every 20 min for a period of 2 h. No additional force was applied using compression bandages.

2.4. ECG recording and analysis

ECG recordings were performed using an MP36R Bio-Pac system (Biopac Systems Inc., CA, USA), with a sampling rate of 1000 Hz, gain of $\times 1000$ and recording time of 1 min. Unmodified Red Dot 2239 wet electrodes were used as controls, and layers of elastic tubular support bandage were used to apply constant force to the electrodes as described above. Three Caucasian male subjects were used, with ages varying from 25 to 31. Appropriate ethical consent was obtained from the subjects and from the Clinical Research Ethics Committee of the Cork Teaching Hospitals (CREC). No skin preparation of any kind was carried out. The electrodes were placed on each arm, below the deltoid muscle or armpit and between the bicep and triceps muscles. The reference electrodes were attached to the left hip, on the waist. Prior to attaching the recording leads, the centres of the microneedle electrodes were lightly tapped to ensure that the electrodes were fully embedded in the skin.

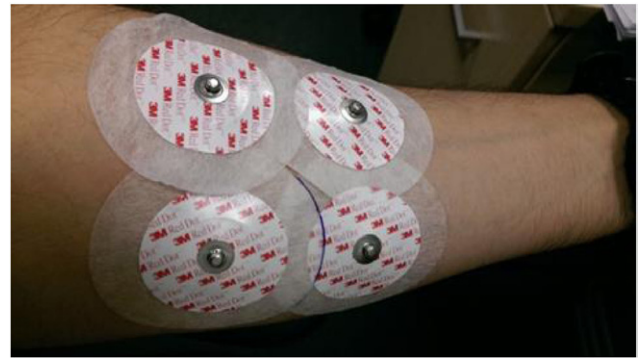


Figure 7. Electrode layout used for impedance recording.

2.5. Signal filtering and SNR analysis

To remove ECG signal artefacts, such as low frequency voltage deviation, random high frequency noise and power line interference, the signal was first digitally filtered off-line in MATLAB using Butterworth infinite impulse response (IIR) 0.05 Hz high pass and 125 Hz low pass filters, and a 50 Hz IIR notch filter.

Assuming that 95% of the noise lies within \pm two standard deviations of the mean value, SNR was then determined using the relationship

$$\text{SNR}_{\text{dB}} = 20 \log \left(\frac{A_{\text{pp}}}{4 \cdot \sigma} \right),$$

where A_{pp} is the peak-to-peak amplitude of the signal R -wave, and σ is the standard deviation of the noise $n(t)$ in the isoelectric region of the ECG signal. This was calculated using the equation

$$n(t) = x(t) - s(t),$$

where $s(t)$ is a signal created by applying a Chebyshev IIR 5th order high pass filter with a cutoff frequency of 50 Hz to the acquired signal $x(t)$. An average value used to determine SNR was obtained by measuring σ at ten locations on each minute-long data recording.

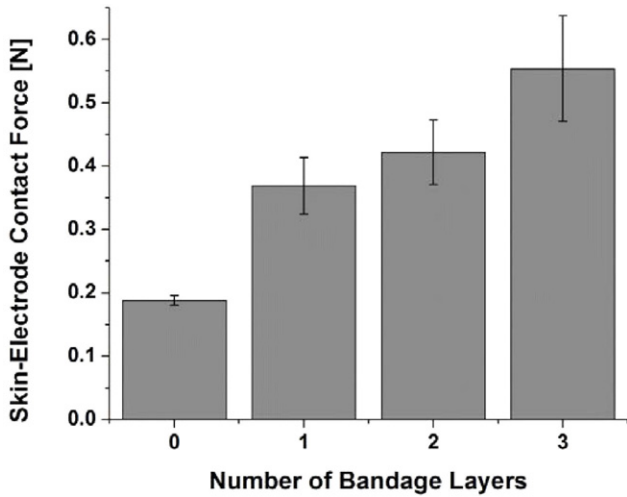


Figure 8. Mean and standard deviation ($\bar{x} \pm S.D.$) of skin electrode contact force ($n = 9$), as a result of applying layers of compression bandage over the electrode.

2.6. Biomechanics

In order to visually assess microneedle penetration efficacy and to confirm that SC breach had taken place, an electrode was applied to the forearm using finger pressure and worn for one minute. After removal, approximately 200 μ l of 1% w/v methylene blue dye was immediately applied to the site and left for 5 min. Excess dye was then removed using a vigorous scrubbing action under cold running water, and the site was examined using a digital microscope (VHX-2000, Keyence Corp., IL, USA).

3. Results

3.1. Application force

Skin-electrode application force is shown in figure 8. The force applied to an electrode by the adhesive backing alone is approximately (0.18 ± 0.1) N, and this may be increased to (0.55 ± 0.08) N by applying three layers of compression bandage over the electrode.

3.2. Variation of skin-electrode impedance with contact force

Figure 9 illustrates the skin-electrode impedance as a function of contact force. It is clear that microneedle electrode impedance decreases significantly as additional force is applied, although the converse effect is not true and a hysteresis-like effect is observed. This is assumed to be due to the embedding of the microneedle structures in the skin, causing penetration of the resistive SC layer and leading to a better electrical contact to the conductive epidermal layers. An increase in force has a much smaller influence on the contact impedance of the flat wet electrode, and skin-electrode impedance remains relatively stable with both increasing and decreasing force.

At the end of the test, the impedance of the wet electrodes is between 30% and 33% lower than that of the microneedle electrodes for all measured frequencies.

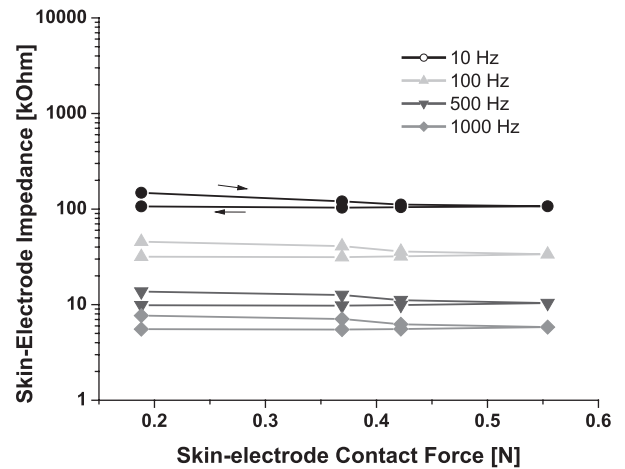
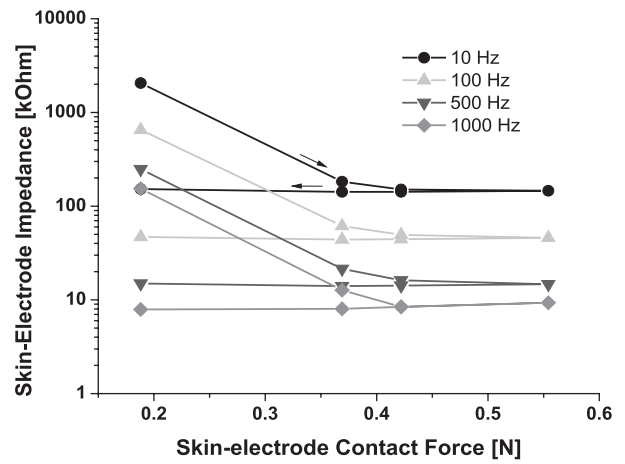


Figure 9. Top: impedance-force curve for microneedle-based dry electrodes. Bottom: impedance-force curve for ‘Red Dot’ wet electrodes.

3.3. Temporal variations in skin-electrode impedance

Figure 10 illustrates the skin-electrode impedance as a function of time; no additional contact force was applied using compression bandages. The skin-electrode impedance decreases slightly over the 2h measurement period for both electrode types.

Analysing these a little more closely, it may be seen from figure 11 that the wet ‘Red Dot’ electrode impedance is initially 25–40% lower than that of the dry microneedle electrodes, data which agrees with that in figure 9 and which is similar to that reported in [26]. However, this discrepancy rapidly decreases, and within an hour the electrode impedances are approximately equal. It is assumed that the variation is due to a buildup of sweat or moisture between the base of the microneedle electrode and the skin, and/or the gradual embedding of the microneedles in the skin. Both effects aid in improving the electrical contact between skin and electrode.

3.4. ECG signal quality

Figure 12 illustrates a typical ECG signal acquired by the microneedle electrodes without additional bandage layers,

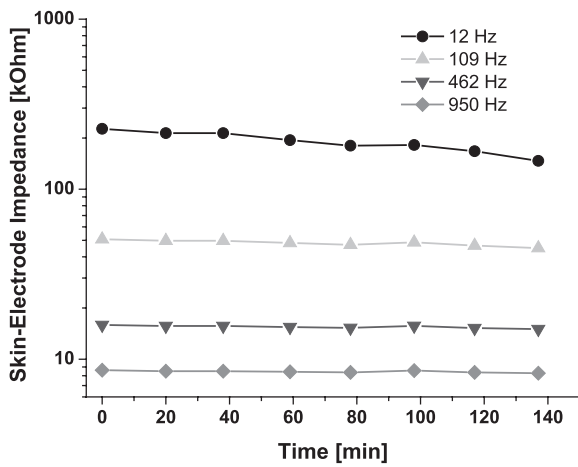
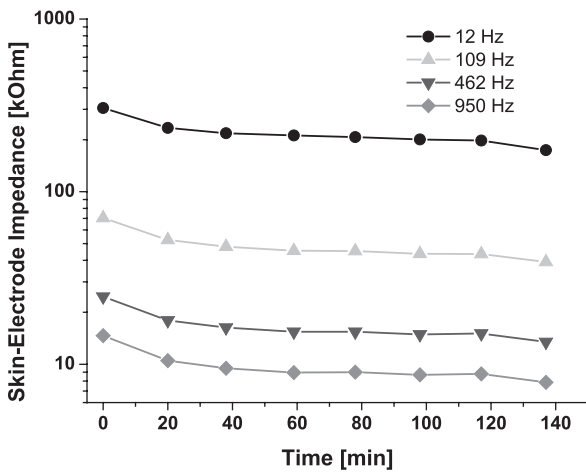


Figure 10. Top: skin-electrode impedance for microneedle-based electrodes as a function of time. Bottom: contact impedance for wet electrodes is slightly more stable than that of dry electrodes.

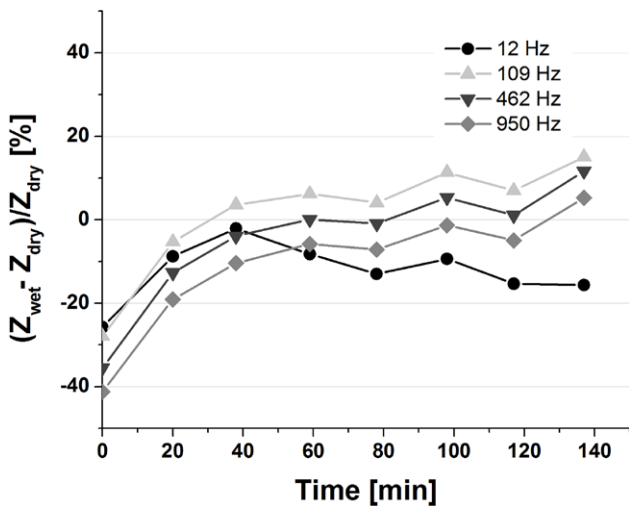


Figure 11. The difference between impedances of the wet and dry electrodes diminishes with time. It is assumed that this effect is due to the gradual embedding of microneedles into skin and/or the buildup of sweat or moisture between the skin and electrode.

i.e. electrode application forces were exerted by the adhesive backing alone (0.18 N, figure 8). The measurements are very similar to those recorded using conventional wet electrodes

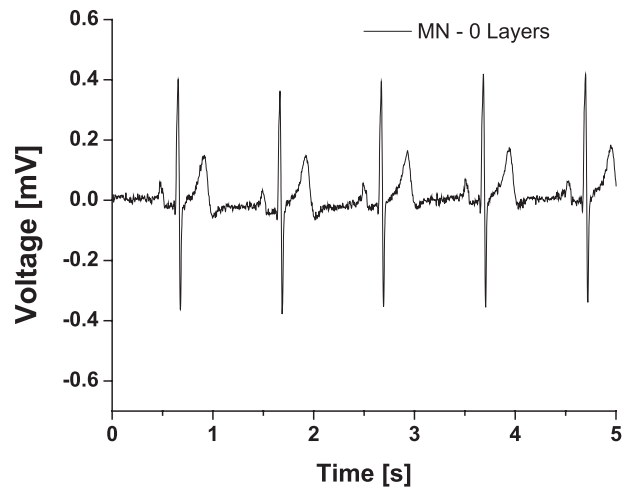


Figure 12. Segment of a 60s ECG recording obtained using a microneedle-based electrode. In this case, no additional contact force was applied via the use of compression bandages.

Table 1. Means and standard deviation ($\bar{x} \pm S.D.$) of filtered SNR, $n = 10$.

Electrode type	Applied force			
	0.18 N (0 layers)	0.37 N (1 layer)	0.42 N (2 layers)	0.55 N (3 layers)
Microneedles	26.0 ± 3.3	26.5 ± 1.2	29.9 ± 1.4	30.3 ± 1.3
Red Dot 2239	27.4 ± 1.3	27.7 ± 1.2	26.8 ± 1.8	26.7 ± 1.0

(data not shown), and the typical cardiac signatures of the P-wave, QRS-complex and T-wave are clearly visible. The heart rate in this case is 62 beats per minute. This proves the ability of dry microneedle-based electrodes manufactured using this process to adequately sense and record ECG signals.

It has also been observed that the noise appears to be reduced by increasing the skin-electrode contact force (data not shown) and this is quantitatively analyzed by examining the SNR of the signals as outlined in section 2.5. The mean SNR of ECG signals collected by microneedle (MN) and wet ‘Red Dot’ (RD) electrodes under increasing contact forces (0–3 layers) are shown in table 1 and were also statistically compared using two-way ANOVA, figure 13.

The differences in SNR between wet and dry electrodes, either affixed to the skin with adhesive backing alone or with one additional bandage layer, are statistically insignificant. However, the use of two or three bandage layers to increase contact force significantly improves the mean SNR of microneedle electrodes ($p < 0.01$).

Additionally, the mean SNR of microneedle electrode recordings with two layers was significantly higher than that of Red Dot electrodes with two and three layers ($p < 0.01$). The mean SNR of microneedle electrode recordings with three layers was also significantly higher than that of all Red Dot traces ($p < 0.01$).

Notably, the SNR of the wet electrode recordings showed no statistically significant improvement when the contact force was increased ($p > 0.05$).

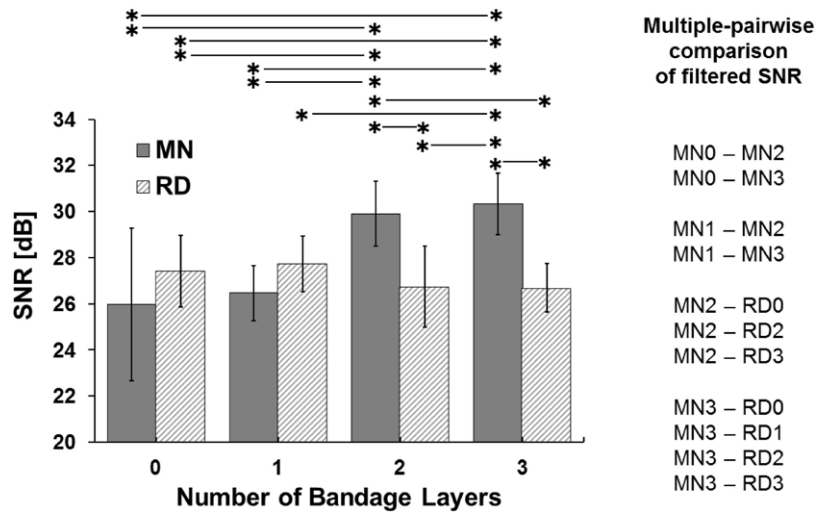


Figure 13. SNR means and standard deviation ($\bar{x} \pm S.D, n = 10$) obtained using microneedle (MN) and commercial Red Dot 2239 (RD) electrodes. Significantly different SNR pairs ($p < 0.01$) are indicated.

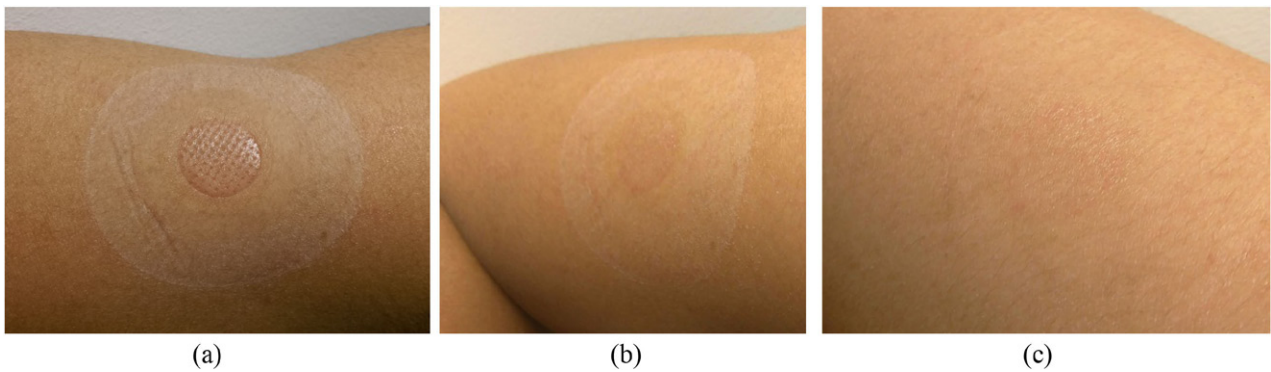


Figure 14. Site of microneedle electrode (a) immediately after removal; (b) 10 min after removal; (c) 30 min after removal.

3.5. Biomechanics

Some study volunteers reported that the application of the microneedle electrodes to the skin can be accompanied by minor, initial discomfort, especially on thin areas overlying bone or areas that flex or stretch during movement (e.g. wrists). The sensation of discomfort subsides in less than 10 min. Application of pressure or any lateral load to the skin-electrode interface can be felt as a very minor stinging sensation. It was observed that the most comfortable area for attaching the electrodes is on the arm, between the triceps, biceps and the deltoid muscles, as this area of the skin undergoes very little distortion during regular movement.

No bleeding or blood spots were observed at any time during application of these 500 μm tall electrodes. Similar to our previous work on silicon electrodes [21] and to that reported by others [33], a well-defined but transient skin erythema, in the shape of the circular array, was observed at the site, figure 14. This fades rapidly and is almost imperceptible one hour after removal.

For comparative purposes, a Red Dot wet electrode was also applied and removed in a similar manner. Transient circular markings due to the adhesive pad are apparent in figure 15 (although the well-defined pattern of dots that results

from the microneedle array are obviously absent), and these fade on a similar timescale to that shown in figure 14.

Skin penetration has been also verified using methylene blue dye, a skin staining agent that has previously been used to indicate the site of microneedle penetration [34, 35]. In this study, staining clearly indicated the presence of conduits formed as a result of microneedle electrode insertion, figure 16. The residual stain marks showed that virtually all of needles present on the electrode array penetrated the SC.

4. Discussion

The use of micromoulding techniques to create low-cost electrodes has several notable advantages over silicon, especially when a double-sided process such as the one outlined here can be used to eliminate post-process via creation and wafer dicing steps. Raw materials are cheap—the cost of the epoxy used in an electrode is no more than a couple of cents, and we have used the silicon master templates to create over 100 elastomeric moulds without any significant degradation of the master or mould. Polymeric materials are less brittle than silicon, and many are already approved for long-term implantation in humans by agencies such as the U.S. Pharmacopeial

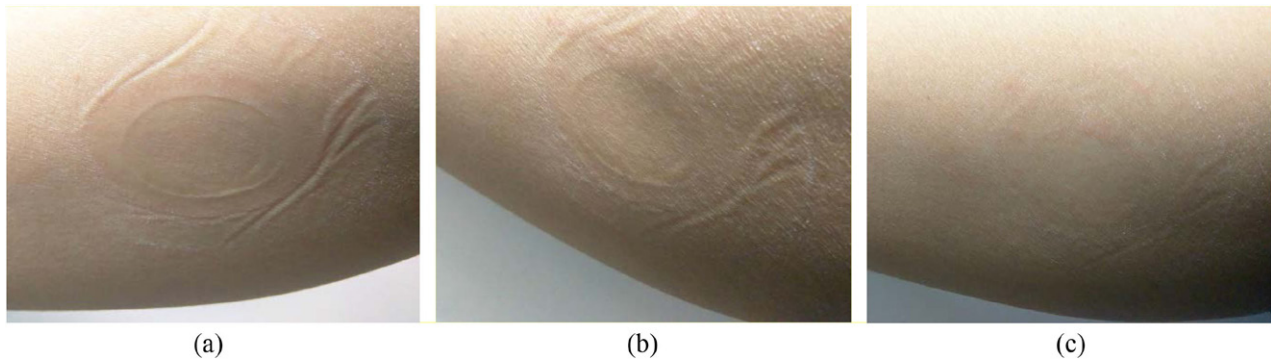


Figure 15. Site of wet electrode (a) immediately after removal; (b) 10 min after removal; (c) 30 min after removal.

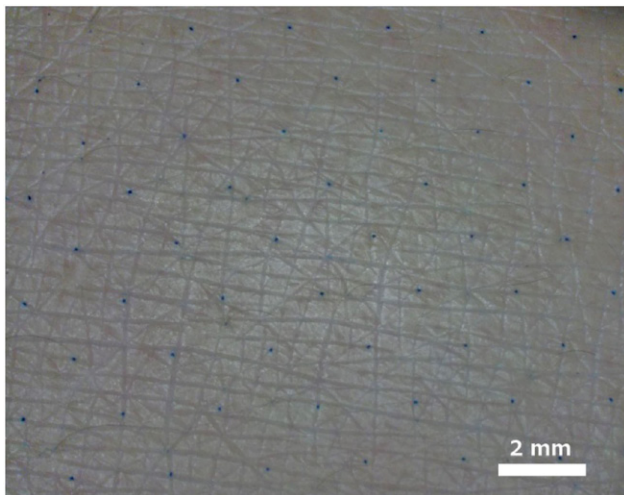


Figure 16. Methylene blue stained pores created by the application of a microneedle electrode to the skin.

Convention (USP). However, polymeric microneedles are usually a little less sharp than their silicon counterparts and have a much lower Young's Modulus. Some materials are therefore prone to suffer minor tip damage during the insertion process, although this may be somewhat irrelevant as the electrodes are intended to be single-use only.

Interestingly, no bleeding is visible after electrode application, even though blood vessels lie much closer to the surface of the skin than the 500 μm needle height [4]. When applied by hand, needle penetration depth is usually less than the needle height—optical coherence tomography imaging has shown that microneedles typically penetrate to around two-thirds of their height, due to compression and deformation of the skin around the needle. Additional deformation of the epidermis around the needle tip further lessens the likelihood of blood vessel rupture taking place [36].

Previous work (data not shown) with similarly-shaped silicon microneedle arrays has demonstrated that blood spots do become visible after application of 800 μm tall microneedles, accompanied with a moderately painful stinging sensation. Combined, these data suggest that 500 μm –600 μm is a reasonable height limit for arrays of this geometry.

Published values for electrode-skin impedance vary widely, primarily due to the large variations in electrode type, geometry and experimental protocols. In general, the impedance

values measured here mimic those reported elsewhere for microneedle devices [5, 27, 28, 30, 37]. Other studies on (non-microneedle) dry electrodes have also observed the effects of pressure on skin-electrode impedance [38], the hysteresis-like effect that results in a sustained decrease in skin-electrode impedance after the loading-unloading cycle shown in figure 9 [39], and the decrease of contact impedance with time as outlined in figure 10 [5, 40, 41]. These effects are attributed to factors such as an increase of contact area with pressure, a buildup of sweat/moisture between skin and electrode, and penetration of the gel electrolyte into the SC layers.

Crucially, the results show that the skin-electrode impedance (and signal quality) of microneedle-based electrodes is a strong function of the contact conditions. In particular, the topography of the microneedle electrodes means that sufficient force must be applied to the electrode in order to embed the microneedles fully in the skin, reduce the skin-electrode impedance and improve the SNR of subsequent recordings. Using new techniques to measure the skin-electrode contact force *in vivo*, this paper has quantified that effect for the first time in such electrodes. The results imply that microneedle-based electrode construction and packaging should incorporate mechanical supports or features (e.g. as suggested in [26]) to assist with consistent application of sufficient contact force.

This work has assessed electrode performance using static subjects. However, future research will also examine the dynamic performance of the electrodes in ambulatory settings. Preliminary reports have already shown that micromachined dry electrodes are capable of reducing the motion artefacts arising from movement of the subject due to the enhanced biomechanical stability associated with anchoring of the needle array in the skin [7, 24, 42]. However, the increased sensitivity of the wet electrode to application pressure that has been demonstrated in this paper further underlines the need for secure skin attachment of the electrode as outlined above.

5. Conclusion

A wafer-level micromoulding process, capable of mass-manufacture of microneedle-based ECG electrodes in high volume and low cost, has been demonstrated. The double-sided process employs two flexible moulds—one to create 500 μm tall microneedle structures on the front side of a polymeric wafer, and a second to simultaneously define through-wafer

electrical vias and circular, detachable arrays on the rear side. This approach reduces fabrication time and complexity by eliminating the additional steps usually required to electrically connect the front and rear of each electrode. It also removes the need for a subsequent wafer dicing step, as the arrays are preformed and easily detached from the polymeric wafer.

For the first time, a study of electrode performance as a function of skin-electrode contact quality has been demonstrated, and new measurement techniques to characterize the skin-electrode electrode application force have been developed. In contrast to conventional wet electrodes, it has been shown that SNR of ECG waveforms acquired using microneedle-based dry electrodes is significantly dependent on the skin-electrode contact force. It is thought that this increase in signal quality with application force is attributable to the decrease in skin-electrode impedance that occurs as skin-electrode contact is improved.

Acknowledgments

This work has been partially supported by Science Foundation Ireland under the INSIGHT Centre, by Enterprise Ireland under the Commercialisation Fund (CF/2012/2339) and the Collaborative Centre for Applied Nanotechnology, by the Higher Education Authority under the Programme for Research in Third-Level Institutions, by the EU Erasmus + mobility scheme, and by Khon Khaen University and the Institute for the Promotion of Teaching Science and Technology of Thailand.

References

- [1] Thakor N V 1998 Biopotentials and electrophysiology measurement *The Measurement, Instrumentation and Sensors Handbook* ed J G Webster (Boca Raton, FL: CRC Press)
- [2] Becker D E 2006 Fundamentals of Electrocardiography Interpretation *Anesth. Prog.* **53** 53–64
- [3] Merletti R 2010 The electrode-skin interface and optimal detection of bioelectric signals *Phys.Meas.* **31** 3
- [4] Tobin D J 2006 Biochemistry of human skin—our brain on the outside *Chem. Soc. Rev.* **35** 52–67
- [5] Searle A and Kirkup L 2000 A direct comparison of wet, dry and insulating bioelectric recording electrodes *Physiol. Meas.* **21** 271
- [6] Liao L-D et al 2011 Design, fabrication and experimental validation of a novel dry-contact sensor for measuring electroencephalography signals without skin preparation *Sensors* **11** 5819–34
- [7] Peng H-L et al 2015 Flexible dry electrode based on carbon nanotube/polymer hybrid micropillars for biopotential recording *Sensors Actuators A* **235** 48–56
- [8] Tam H and Webster J G 1977 Minimizing electrode motion artifact by skin abrasion *IEEE Trans. Biomed. Eng.* **BME-24** 134–9
- [9] 2001 3M, *FAQ-Electrodes* (<http://multimedia.3m.com/mws/media/1339030/faqs-electrodes.pdf>)
- [10] Chang C L et al 2010 A power-efficient bio-potential acquisition device with DS-MDE sensors for long-term healthcare monitoring applications *Sensors* **10** 4777–93
- [11] Taheri B A, Knight R T and Smith R L 1994 A dry electrode for EEG recording *Electroencephalogr. Clin. Neurophysiol.* **90** 376–83
- [12] Kim Y-C, Park J-H and Prausnitz M R 2012 Microneedles for drug and vaccine delivery *Adv. Drug Deliv. Rev.* **64** 1547–68
- [13] van der Maaden K, Jiskoot W and Bouwstra J 2012 Microneedle technologies for (trans) dermal drug and vaccine delivery *J. Control. Rel.* **161** 645–55
- [14] Griss P et al 2001 Micromachined electrodes for biopotential measurements *J. Microelectromech. Syst.* **10** 10–6
- [15] Griss P et al 2002 Characterization of micromachined spiked biopotential electrodes *IEEE Trans. Biomed. Eng.* **49** 597–604
- [16] Haq M et al 2009 Clinical administration of microneedles: skin puncture, pain and sensation *Biomed. Microdevices* **11** 35–47
- [17] Donnelly R F et al 2009 Microneedle arrays allow lower microbial penetration than hypodermic needles *in vitro Pharm. Res.* **26** 2513–22
- [18] Wang Y et al 2011 Fabrication of dry electrode for recording bio-potentials *Chin. Phys. Lett.* **28** 010701
- [19] Guo D G et al 2008 A wearable BSN-based ECG-recording system using micromachined electrode for continuous arrhythmia monitoring *5th Int. Summer School and Symp. on Medical Devices and Biosensors (ISSS-MDBS 2008)* pp 41–4
- [20] Swaminathan R et al 2011 Micromachined three-dimensional electrode arrays for transcutaneous nerve tracking *J. Micromech. Microeng.* **21** 085014
- [21] O'Mahony C et al 2012 Microneedle-based electrodes with integrated through-silicon via for biopotential recording *Sensors Actuators A* **186** 130–6
- [22] O'Mahony C et al 2013 Skin insertion mechanisms of microneedle-based dry electrodes for physiological signal monitoring *2013 IEEE Biomedical Circuits and Systems Conf. (BioCAS) (Rotterdam)* (IEEE) pp 69–72
- [23] Matteucci M et al 2007 Micropatterned dry electrodes for brain-computer interface *Microelectron. Eng.* **84** 1737–40
- [24] Forvi E et al 2012 Preliminary technological assessment of microneedles-based dry electrodes for biopotential monitoring in clinical examinations *Sensors Actuators A* **180** 177–86
- [25] Choi S O et al 2010 An electrically active microneedle array for electroporation *Biomed. Microdevices* **12** 263–73
- [26] Srivastava A K et al 2015 Long term biopotential recording by body conformable photolithography fabricated low cost polymeric microneedle arrays *Sensors Actuators A* **236** 164–72
- [27] Miyako A, Yuya N and Norihisa M 2015 Electroencephalogram measurement using polymer-based dry microneedle electrode *Japan. J. Appl. Phys.* **54** 06FP14
- [28] Wang L-F et al 2013 A MEMS-based pyramid micro-needle electrode for long-term EEG measurement *Microsyst. Technol.* **19** 269–76
- [29] Kommareddy S et al 2014 Influenza subunit vaccine coated microneedle patches elicit comparable immune responses to intramuscular injection in guinea pigs *Vaccine* **31** 3435–41
- [30] Hsu L-S et al 2014 Developing barbed microtip-based electrode arrays for biopotential measurement *Sensors* **14** 12370–86
- [31] Wilke N and Morrissey A 2007 Silicon microneedle formation using modified mask designs based on convex corner undercut *J. Micromech. Microeng.* **17** 238
- [32] Tekscan, Inc. 2010 *FlexiForce Sensors Users Manual* (Boston, MA: Tekscan Inc.)
- [33] Kim M et al 2015 Curved microneedle array-based sEMG electrode for robust long-term measurements and high selectivity *Sensors* **15** 16265
- [34] Li W Z et al 2010 Super-short solid silicon microneedles for transdermal drug delivery applications *Int. J. Pharm.* **389** 122–9
- [35] O'Mahony C 2014 Structural characterization and *in vivo* reliability evaluation of silicon microneedles *Biomed. Microdevices* **6** 333–43
- [36] Enfield J et al 2010 *In vivo* dynamic characterization of microneedle skin penetration using optical coherence tomography *J. Biomed. Opt.* **15** 046001

- [37] Roxhed N *et al* 2007 Penetration-enhanced ultrasharp microneedles and prediction on skin interaction for efficient transdermal drug delivery *J. Microelectromech. Syst.* **16** 1429–40
- [38] Taji B *et al* 2014 Impact of skin-electrode interface on electrocardiogram measurements using conductive textile electrodes *IEEE Trans. Instrum. Meas.* **63** 1412–22
- [39] Albulbul A and Chan A D C 2012 Electrode-skin impedance changes due to an externally applied force *2012 IEEE Int. Symp. on Medical Measurements and Applications Proc. (MeMeA) (Budapest)* (IEEE) pp 1–4
- [40] Baba A and Burke M 2008 Measurement of the electrical properties of ungelled ECG electrodes *Int. J. Biol. Biomed. Eng.* **2** 89–97
- [41] Gruetzmann A, Hansen S and Müller J 2007 Novel dry electrodes for ECG monitoring *Physiol. Meas.* **28** 1375
- [42] Zhang H, Pei W, Chen Y, Guo X, Wu X, Yang X and Chen H 2015 A motion interference-insensitive flexible dry electrode *IEEE Trans. Biomed. Eng.* pp 1136–44